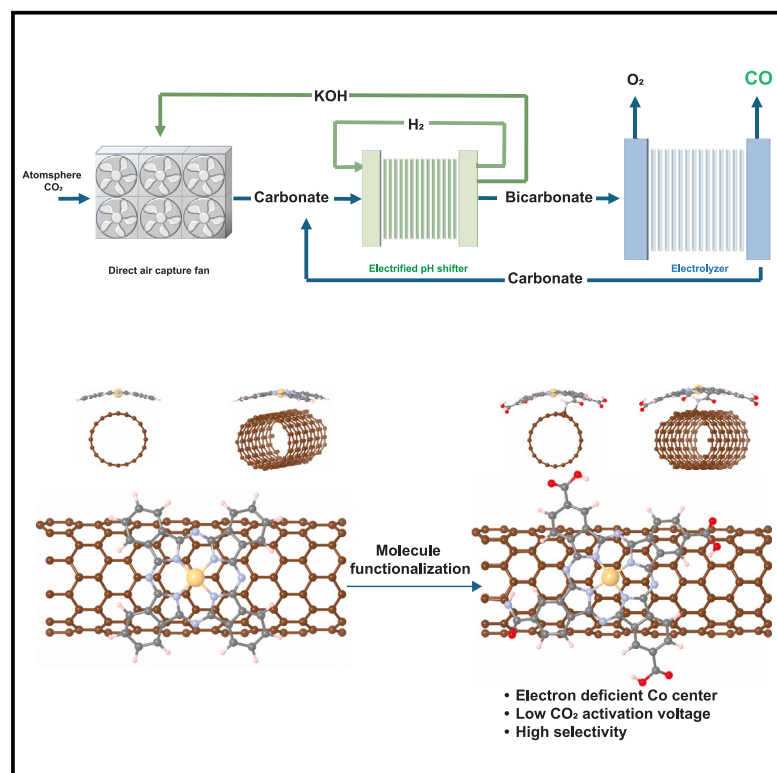


# Electrosynthesis of CO from an electrically pH-shifted DAC post-capture liquid using a catalyst: support amide linkage

## Graphical abstract



## Authors

Bei Zhou, Hengzhou Liu, Guangcan Su, ..., Pengfei Ou, Ke Xie, Edward H. Sargent

## Correspondence

ke-xie@northwestern.edu (K.X.), ted.sargent@northwestern.edu (E.H.S.)

## In brief

Electrified reactive capture integrates CO<sub>2</sub> capture and conversion into a single process, offering an energy-efficient alternative to sequential DAC, release, and upgrade. We implement a pH-downshifter to convert carbonate from the post-DAC liquid to bicarbonate. By functionalizing a CoPc catalyst with support effects, we lower the bicarbonate electrolysis cell voltage and improve selectivity to CO. Our approach contributes to a path toward more efficient air-to-chemicals conversion.

## Highlights

- pH downshift enhances CO<sub>2</sub> availability for efficient electrolysis
- CoPc functionalization lowers overpotential and enhances CO production efficiency
- Regeneration of capture medium is demonstrated

## Article

# Electrosynthesis of CO from an electrically pH-shifted DAC post-capture liquid using a catalyst: support amide linkage

Bei Zhou,<sup>1,3</sup> Hengzhou Liu,<sup>1,3</sup> Guangcan Su,<sup>1</sup> Heejong Shin,<sup>1</sup> Xiao-Yan Li,<sup>1</sup> Huajie Ze,<sup>1</sup> Yongxiang Liang,<sup>1</sup> Bosi Peng,<sup>1</sup> Weiyan Ni,<sup>1</sup> Yuanjun Chen,<sup>1</sup> Wenjin Zhu,<sup>1</sup> Christine Yu,<sup>1</sup> Yiqing Chen,<sup>1</sup> Pengfei Ou,<sup>1,2</sup> Ke Xie,<sup>1,2,\*</sup> and Edward H. Sargent<sup>1,2,4,\*</sup>

<sup>1</sup>Department of Chemistry, Northwestern University, 2145 Sheridan Road, Evanston, IL 60208, USA

<sup>2</sup>Department of Electrical and Computer Engineering, Northwestern University, 2145 Sheridan Rd., Evanston, IL 60208, USA

<sup>3</sup>These authors contributed equally

<sup>4</sup>Lead contact

\*Correspondence: [ke-xie@northwestern.edu](mailto:ke-xie@northwestern.edu) (K.X.), [ted.sargent@northwestern.edu](mailto:ted.sargent@northwestern.edu) (E.H.S.)

<https://doi.org/10.1016/j.joule.2025.101883>

**CONTEXT & SCALE** Direct air capture (DAC) of CO<sub>2</sub> is a technology of interest for supplying a feedstock for ensuing CO<sub>2</sub> utilization; yet systems demonstrated to date are energy intensive. One promising approach is electrified reactive capture, where CO<sub>2</sub> absorbed in an alkali carbonate solution is electrochemically converted to value-added intermediates such as CO, simultaneously regenerating the capture medium. However, prior studies have typically required energy intensities exceeding 59 GJ/ton CO, linked to high cell potentials (full-cell voltage > 3.7 V) and limited CO selectivity (<45%). In this work, we studied how to increase activity in bicarbonate electrolysis toward CO; we found a molecular catalyst substitution strategy to be effective, one in which tuning the electronic environment of a cobalt-based catalyst lowered the activation energy on the path to CO<sub>2</sub> conversion. We grafted the catalyst covalently onto a conductive carbon nanotube support with the aid of amide linkages, and we found this to improve charge transfer and reaction kinetics. In the system, we introduced an electrified pH-downshifter in order to increase CO<sub>2</sub> availability in the reactive capture phase. As a result, we report bicarbonate electrolysis to CO that requires a full-cell voltage of 2.7 V (100 mA cm<sup>-2</sup>) and provides 70% faradaic efficiency, resulting in an energy intensity of 35 GJ/ton CO. This energy budget is comparable to that needed in DAC followed by reverse water-gas shift (RWGS), which requires high-temperature (~800°C) thermocatalysis. The present system, operating as it does at ambient conditions, offers simplification and modularization of atmospheric-CO<sub>2</sub>-to-concentrated-CO production.

## SUMMARY

Electrified reactive capture upgrades CO<sub>2</sub> from post-air-capture alkali carbonate liquid to value-added products while regenerating the capture medium. Previous processes exhibited limited energy efficiency (<18%) due to high full-cell voltage (>3.7 V) and modest CO selectivity (<45%). To address this, we developed a Co molecular catalyst featuring an electron-deficient Co center, lowering the required reduction voltage. We then grafted the catalyst onto a conductive support, enhancing charge transfer. An electrified pH-downshifter improved CO<sub>2</sub> availability, increasing CO selectivity. The system achieved 70% CO selectivity at 2.7 V and 100 mA cm<sup>-2</sup>, corresponding to an energy intensity of 35 GJ/ton CO. The energy cost is comparable to that of direct air capture (DAC) followed by reverse water-gas shift (RWGS), but it offers ambient temperature operation.

## INTRODUCTION

CO<sub>2</sub> capture from the atmosphere, paired with the renewable electricity-powered synthesis of CO and subsequent processing to hydrocarbons, has the potential to reduce the carbon intensity of fuels.<sup>1-4</sup>

Air-to-concentrated-CO conversion can be accomplished by sequencing direct air capture (DAC) with gas-fed CO<sub>2</sub> electrolysis.<sup>5-7</sup> One cost-effective and scalable DAC system uses alkali hydroxide (e.g., KOH) solution to turn CO<sub>2</sub> into carbonate, followed by a calcium loop to regenerate hydroxide and release concentrated CO<sub>2</sub>.<sup>8-10</sup> The calcium loop involves a calcination



process operating at  $\sim 900^\circ\text{C}$ , consuming 6–10 GJ/ton  $\text{CO}_2$ , adding a minimum of 10–16 GJ/ton CO for the supply of the carbon feedstock (1.6 tons of  $\text{CO}_2$  is needed per ton CO at best-case 100% atom efficiency). In view of the 10.1 GJ/ton lower heating value of CO, this is a significant upfront penalty.

Work on reactive capture posits that  $\text{CO}_2$  regeneration and upgrade (such as carbonate into CO on the cathode; plus hydroxide for recycling into the capture unit) could potentially be integrated for a beneficial effect.<sup>2,11,12</sup> Hydroxide can be isolated from CO in a knockout drum and fed back to the contactor for the capture of the next batch of atmospheric  $\text{CO}_2$ . By avoiding the thermal regeneration of the capture medium and by simplifying aspects of  $\text{CO}_2$  purification and compression, reactive capture can potentially reduce operating and capital expenditures when one examines the complete chain from (dilute) atmospheric  $\text{CO}_2$  to substantially pure CO.<sup>13</sup>

For the kinetics and capital efficiency of the contactor to provide practical DAC, the KOH in contact with  $\text{CO}_2$  can be progressively loaded with carbon down to the pH of potassium carbonate ( $\text{K}_2\text{CO}_3$ ), pH 12; after this pH, estimates indicate that the kinetics of capture become so low that the contactor (fan) energy and capital infrastructure become too costly.<sup>14</sup> Yet, in the second step—the electrolysis of the post-capture liquid to CO—the use of carbonate as feedstock leads to faradaic efficiencies (FEs) in the range of 25%<sup>15</sup> to 40%,<sup>16</sup> when silver nanoparticles are employed, with typical cell voltages of 3.3–3.8 V at 100–200  $\text{mA cm}^{-2}$  current density. In contrast to bicarbonate, FE has reached the 80%–90% range when Co<sup>17</sup> and Ni-based<sup>18</sup> single-atom catalysts are employed.

We therefore explored the use of a fully electrified system (Figure 1A) comprising a first stage that downshifts pH to that of bicarbonate and then reduces  $\text{CO}_2$  to CO from this liquid.

The full-cell voltage of the most energy-efficient prior bicarbonate electrolyzers has typically resided in the range of 3.2–3.8 V at a current density of 100  $\text{mA cm}^{-2}$ .<sup>14,18</sup> Thus, we herein focus on reducing the cell voltage as a major priority.

## RESULTS AND DISCUSSION

### Functionalized molecular catalysts

The cathodic overpotential for  $\text{CO}_2$  activation, a major contributor to cell voltage, can potentially be lowered by electronic tuning; here, we focused on cobalt phthalocyanine (CoPc), known for providing  $\text{CO}_2$ -to-CO conversion<sup>19–24</sup> and having a molecular structure that allows the introduction of functional groups to manipulate its electronic properties.

We studied functionalizing CoPc with electron-donating (amino-CoPc on carbon nanotube [CNT], denoted “amino-CoPc/CNT”) and electron-withdrawing (carboxylate CoPc-on-CNT, denoted “carboxylate”) groups, aiming to modulate the electronic state of the cobalt center. We deposited these functionalized molecules on CNTs and then also studied chemical linkages between CoPc and the CNT support.

To gain an initial assessment of the impact of functional groups on the Co center of CoPc, we used density functional theory (DFT): the Bader charge on the Co sites in Figure 1B shows that carboxylate induces electron depletion on the Co center, whereas amine groups induce electron-rich conditions.

We screened bicarbonate electrolysis performance in a two-electrode membrane electrode assembly (MEA) electrolyzer using a commercial bipolar membrane (BPM); an 85- $\mu\text{m}$ -thick polytetrafluoroethylene (PTFE) porous interposer layer was sandwiched between BPM and the cathode. We observed that (Figure 2A) carboxylate lowers overpotential while amino-CoPc/CNT has little effect on overpotential. Neither functionalization enhances CO selectivity, compared with “control” that does benefit from CoPc molecular functionalization (Figure 2B); they all show a similar  $\text{FE}_{\text{CO}}$  of 46%–51% at 100  $\text{mA cm}^{-2}$ .

We hypothesized that CO selectivity might be improved if we could achieve efficient charge transfer between CNT support and the cobalt center. A covalent bond, such as an amide linkage, between functional groups on the CNT support and the CoPc could potentially achieve this goal.

We sought therefore to graft the carboxylate-modified CoPc onto amine-modified CNT substrates, where we anticipated that carboxylate would anchor to amine via  $\pi$ - $\pi$  interactions; and a covalent bond form between carboxyl and amine functional groups after heating.<sup>25</sup> The formation of the amide bond is evidenced in the N 1s X-ray photoelectron spectroscopy (XPS) profile in Figure S3. Compared with the mixture (without heating) of carboxylate-modified CoPc and amine-modified CNT, heat treatment shifts the N signal to a lower binding energy, indicating that the extent of electron deficiency of phthalocyanine-N is diminished by the formation of the amide bond. High-resolution transmission electron microscopy (HRTEM) and associated energy-dispersive X-ray spectroscopy (EDS) (Figure S4) indicate that carboxylate CoPc has been loaded onto amine CNTs.

This class of samples we term “amide” (CoPc–COOH bond on CNT-NH<sub>2</sub>). They show a similarly low overpotential to that of carboxylate (Figure 2A).

However, amide simultaneously shows an increased  $\text{FE}_{\text{CO}}$  (Figure 2B) of  $\sim 70\%$  at 100  $\text{mA cm}^{-2}$ ; indeed, it maintains this FE at 150  $\text{mA cm}^{-2}$  and remains above 60% up to 300  $\text{mA cm}^{-2}$ . We prepared a CoPc-COOH on CNT-NH<sub>2</sub> sample without the formation of amide bonding (denoted “no-linkage”) and recorded an  $\text{FE}_{\text{CO}} < 40\%$  (Figure 2B). Also, the CoPc-on-CNT-NH<sub>2</sub> (denoted amine) shows an insignificant change in  $\text{FE}_{\text{CO}}$  (Figure 2B). These results highlight the critical role of amide bonding.

### Mechanistic studies

Cyclic voltammograms (CVs) were used to study the mechanism. We compared CoPc with/without functional groups, finding that in an Ar-saturated electrolyte, all samples showed a reversible redox couple between 0.048 and 0.266 V, assigned to the  $\text{Co}^{\text{II}}/\text{Co}^{\text{I}}$  redox.<sup>23</sup>  $\text{Co}^{\text{II}}$  needs to transform to  $\text{Co}^{\text{I}}$  to be active for  $\text{CO}_2$  reduction.<sup>26</sup> Among these samples, carboxylate show a positive shift of its  $\text{Co}^{\text{II}}/\text{Co}^{\text{I}}$  redox peaks (Figure 3A), compared with control, implying that the –COOH groups on the Pc ligand withdraw the electron from the cobalt center. In contrast, the  $\text{Co}^{\text{II}}/\text{Co}^{\text{I}}$  redox of amino-CoPc/CNT shows a negative shift, compared with control, as well as compared with carboxylate. This result is consistent with their similar cell voltage trend (Figure 2A), with the contention that the electron-withdrawing characterization is linked to the overpotential reduction in these materials. We compared  $\text{CO}_2\text{R}$  activities through linear

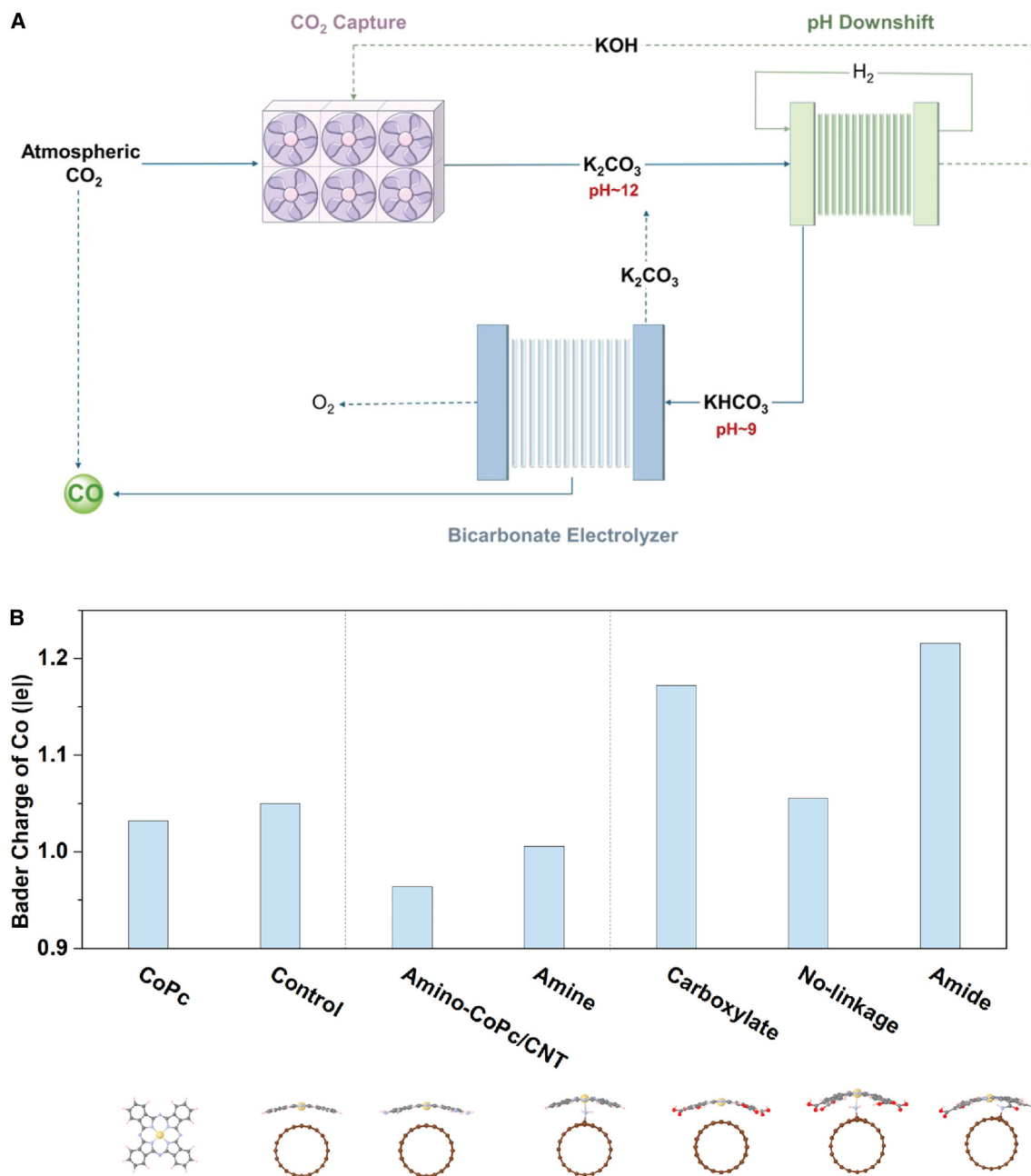


**Figure 1. Electronic structure of CoPc modulated via the addition of different functional groups**

(A) Reactive capture system integrating a pH-downshifter based on internal hydrogen looping.

(B) Calculated Bader charges of the Co sites in CoPc, CoPc-on-CNT (denoted control), amino-CoPc on CNT (denoted amino-CoPc/CNT), CoPc-on-CNT-NH<sub>2</sub> (denoted amine), carboxylate CoPc-on-CNT (denoted carboxylate), CoPc-COOH on CNT-NH<sub>2</sub> without amide bond (denoted no-linkage), and CoPc-COOH bond on CNT-NH<sub>2</sub> (denoted amide). A higher value represents a great degree of electron deficiency. The corresponding atomic structure models are shown at the bottom.

sweep voltammetry (LSV) potentials (Figures 3C and S6) under CO<sub>2</sub> vs. N<sub>2</sub> atmospheres. These agree well with the trend of cell voltage in MEA (Figure 2A). In CO<sub>2</sub>, amide displays a lower potential at 10 mA cm<sup>-2</sup>. In the N<sub>2</sub> atmosphere, amide shows a higher hydrogen evolution reaction (HER) potential, compared with that in CO<sub>2</sub> atmosphere, indicating faster CO<sub>2</sub> reduction ki-

netics compared with those for HER. In contrast, carboxylate shows similar potentials in CO<sub>2</sub> and N<sub>2</sub> atmospheres. These results are in accord with the observed higher FE<sub>CO</sub> of amide.

We used *operando* Raman spectroscopy (Figures 3D–3G) to probe the transformation from Co<sup>II</sup> (Raman shift: 754 cm<sup>-1</sup>) to Co<sup>I</sup> (Raman shift: 747 cm<sup>-1</sup>).<sup>26</sup> For amide, carboxylate, and

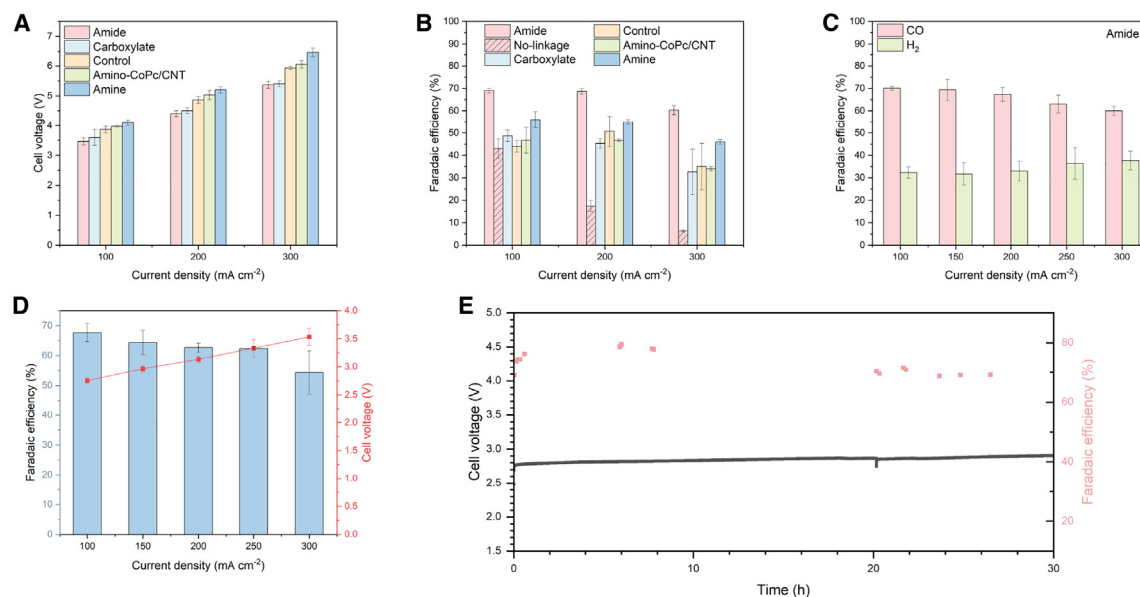


**Figure 2. Bicarbonate electrolysis performance as a function of functional group selection on CoPc and CNTs**

(A) Cell voltage comparison of different CoPc catalysts, where a commercial BPM + Ni foam anode were employed; (B) catalyst screening and performance comparison for different CoPc catalysts; (C)  $FE_{CO}$  of CoPc-COOH bond on CNT-NH<sub>2</sub> (amide) at different current densities; (D)  $FE_{CO}$  and cell voltage using synthetic BPM and NiFeOx anode; (E) stability test during bicarbonate electrolysis over the course of continuous operation at 100 mA cm<sup>-2</sup>. Experiments were conducted in N<sub>2</sub>-saturated 3 M KHCO<sub>3</sub>. An 85- $\mu$ m-thick PTFE porous interposer layer was sandwiched between BPM and cathode. All the error bars represent the standard deviation of three measurements.

amine, Co<sup>II</sup> starts to transform to Co<sup>I</sup> at 0.16 V vs. RHE but only at -0.04 V vs. RHE for control. At 0.16 V vs. RHE, a higher Co<sup>I</sup>:Co<sup>II</sup> ~ 3.2 was observed for amide, while the value was 2.2 for carboxylate and 0.5 for amine. At -0.04 V vs. RHE, the transformation of Co<sup>II</sup> to Co<sup>I</sup> is more complete in amide than in the other catalysts, as evidenced from the higher Co<sup>I</sup>:Co<sup>II</sup> ratio of 30, compared with carboxylate (3.1) and amine (11.6). At a more negative potential of -0.24 V vs. RHE, Co<sup>I</sup> was the dominant species with no observable Co<sup>II</sup> in all samples. The Raman results align with the CV data (Figures 3A and 3B), indicating that the trend in the Co<sup>II</sup> to Co<sup>I</sup> transformation follows an order of increasing difficulty: amide (most facile) < carboxylate < amine < control (most difficult).

These results agreed with CV studies (Figures 3A and 3B) that also indicated that amide enables the Co center to be more easily reduced to Co<sup>I</sup>. We propose that an electron-deficient nature contributes to CO<sub>2</sub> reduction at a lowered overpotential.

### System demonstration

To build a full cell, we employed a NiFeOx electrode and a BPM using TiO<sub>2</sub> as the water dissociation catalyst to pursue a lower  $V_{cell}$ , and we achieved 2.7 V at 100 mA cm<sup>-2</sup> (Figure 2D). We evaluate the contribution of each electrolyzer component to the cell voltage in Figure S7. We also optimized the interposer layer to maximize  $FE_{CO}$  (Figure S8).

We studied the durability of this bicarbonate electrolyzer by observing its continuous operation at a current density of 100 mA cm<sup>-2</sup>. We found that 70%  $FE_{CO}$  is maintained over 30 h (Figure 2E). In a number of prior reports on electrochemical reactive capture,<sup>15,16</sup> carbonate-rich post-capture liquid is fed into a BPM-based electrolyzer, where the carbonate is turned into

CO<sub>2</sub> and reduced to products. Here, we add at the front end a subsystem (pH-downshifter) (Figure 1A) to vary the solution for electrolysis between the pH of post-capture solution of ~12 and that of bicarbonate of ~9. The lower pH promotes *i*-CO<sub>2</sub> availability but consumes more pH-downshifter electricity. We therefore evaluated the electricity consumption of each step with various pH-downshifter effluent pHs.

We used an electrochemical hydrogen looping device (Figure S10) in the downshifter: the anode oxidizes hydrogen and generates protons, partially acidifying the solution flowing in the slim flow chamber; potassium migrates through the cation exchange membrane to the cathode, combining with the OH<sup>-</sup> generated from the HER. It thus outputs KOH solution ready for reuse as DAC sorbent in the contactor upstream. Hydrogen produced from the cathode is fed to the anode for continuous operation.

We fed the pH-downshifter using a simulated post-capture liquid consisting of 1.5 M K<sub>2</sub>CO<sub>3</sub> solution and monitored the anolyte pH (and thus carbonate:bicarbonate relative composition) as well as the cell voltage (Figure 4A). The device converted 93% of carbonate to bicarbonate for the case of final pH ~ 9, and it consumes 3.8 GJ/ton CO<sub>2</sub> (hence ~6 GJ/ton CO) of electricity in so doing (details see Note S1). In parallel, KOH is regenerated in the catholyte, closely approaching the stoichiometry of generated bicarbonate.

We performed continuous bicarbonate electrolysis using the pH ~ 9 post-pH-downshift solution as the feedstock. The change of pH and the corresponding (b)carbonate concentrations are shown vs. elapsed time in Figure 4B. From these, we conclude that dissolved inorganic carbon was converted to

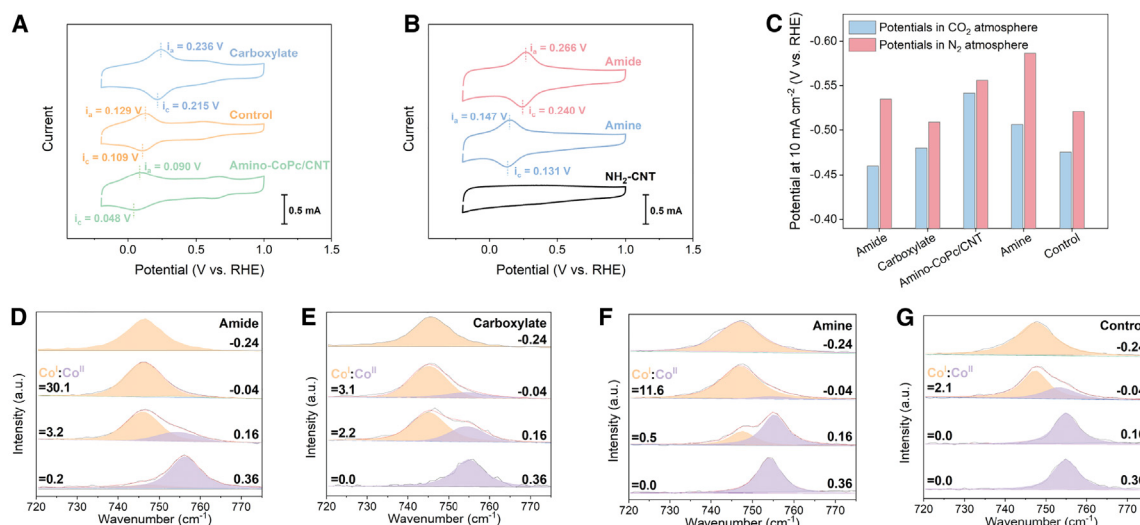


**Figure 3. Electronic tuning of functionalized CoPc/CNT samples**

(A and B) Cyclic voltammograms (CVs) of different CoPc molecules and CNT support combinations, all in a 3 M KHCO<sub>3</sub> solution saturated with Ar. The dotted lines indicate the Co<sup>II</sup>/Co<sup>I</sup> redox reaction in CoPc.

(C) The potentials (at 10 mA cm<sup>-2</sup>) obtained from LSV of different CoPc molecules and CNT supports in a 3 M KHCO<sub>3</sub> solution saturated with CO<sub>2</sub> and N<sub>2</sub>. The LSV profiles are shown in Figure S6.

(D–G) *In situ* Raman spectra of amide, carboxylate, amine, and control in 3 M KHCO<sub>3</sub>. *In situ* analysis was performed in a flow cell having three compartments. Materials were coated on hydrophobic carbon paper as the cathode, with a Pt wire serving as anode. All potentials are referenced to reversible hydrogen electrode (RHE).

CO, while carbonate was delivered at the liquid phase outlet of the system. This post-electrolysis solution was again input into the pH-downshifter to get back to pH ~ 9, and CO production is again demonstrated; see Note S4 for details.

Looking at the full process, we found that since (bi)carbonate electrolysis dominates overall energy consumption, and since bicarbonate electrolysis is much more efficient than carbonate electrolysis, it makes sense to shift all the way to bicarbonate pH 8.8. In this case, the electrolysis energy is 25 GJ/ton CO, and the total—inclusive of pH downshift—is 35 GJ/ton CO. When one compares this (Figure 4D; details in Note S1) with alternatives such as thermal release (calcium looping) to produce concentrated gas-phase CO<sub>2</sub>, followed by either gas-phase CO<sub>2</sub> coelectrolysis or reverse water-gas shift (RWGS), we find the present experimental data to approach closely those of the most-efficient contender, the DAC + RWGS system.

We forecast additional ways to improve the energy efficiency of the bicarbonate electrolyzer and the pH-downshifter. If the bicarbonate electrolyzer can reach FE<sub>CO</sub> of 93%, cell voltage of 2.3 V, and a pH-downshifter energy of 4.5 GJ/ton CO, then CO could be delivered at as little as 25 GJ/ton CO. This will require further work on catalysts, membranes, and electrolyzers. We provide a life cycle assessment (LCA) and techno-economic analysis (TEA) comparing CO production approaches (Note S2). The capital expenditure for the pH-downshifter is the largest cost component of the present production approach (~\$200/ton CO, 25% of the total CO production cost), a consequence of the low 25 mA cm<sup>-2</sup> current density and the opportunity to improve further the energy efficiency (6 GJ/ton CO) of this step. When further

progress enables 50 mA cm<sup>-2</sup> and higher efficiency (4.5 GJ/ton CO), the cost will be reduced to ~\$75/ton CO.

In this work, we demonstrate that a pH-downshifter converts pH 12 post-capture liquid to pH 9, in which electrolysis to CO has an FE of ~70%. CO<sub>2</sub> capture is best done using a pH 13–14 solution, but reactive capture is best done at pH 9. For the kinetics and capital efficiency of the contactor to provide practical DAC, the capture liquid is in the range of pH 14 (at the start of capture) down to pH 13.5 (at the outlet of the contactor) in the calcium loop.<sup>8</sup> Further contacting down to pH 12 (carbonate) requires extra fan energy, while electrochemically down shifting pH 13.5 to pH 12 also requires extra electricity. Additional work in reactive capture can investigate further the amount of dissolved inorganic carbon in the post-capture liquid, pursue further decrease in the pH-downshifter electricity consumption, and seek to increase further the electrolyzer energy efficiency.

## Conclusions

In this work, we applied a pH-downshift strategy to enable high CO production performance from atmosphere CO<sub>2</sub> via reactive capture. We improved bicarbonate reduction efficiency at a lowered overpotential by jointly tuning the properties of CoPc catalyst and support by COOH-functionalized CoPc and anchoring it to a –NH<sub>2</sub>-modified CNT support. We converted a post-capture liquid (pH ~ 12) to KHCO<sub>3</sub> (pH ~ 9) in an electrified pH-downshifter, and then we performed reactive capture with ~70% FE<sub>CO</sub> at 2.7 full-cell voltage at 100 mA cm<sup>-2</sup>. The bicarbonate electrolysis subsystem showed stability for 30 h under continuous operation at 100 mA cm<sup>-2</sup>.

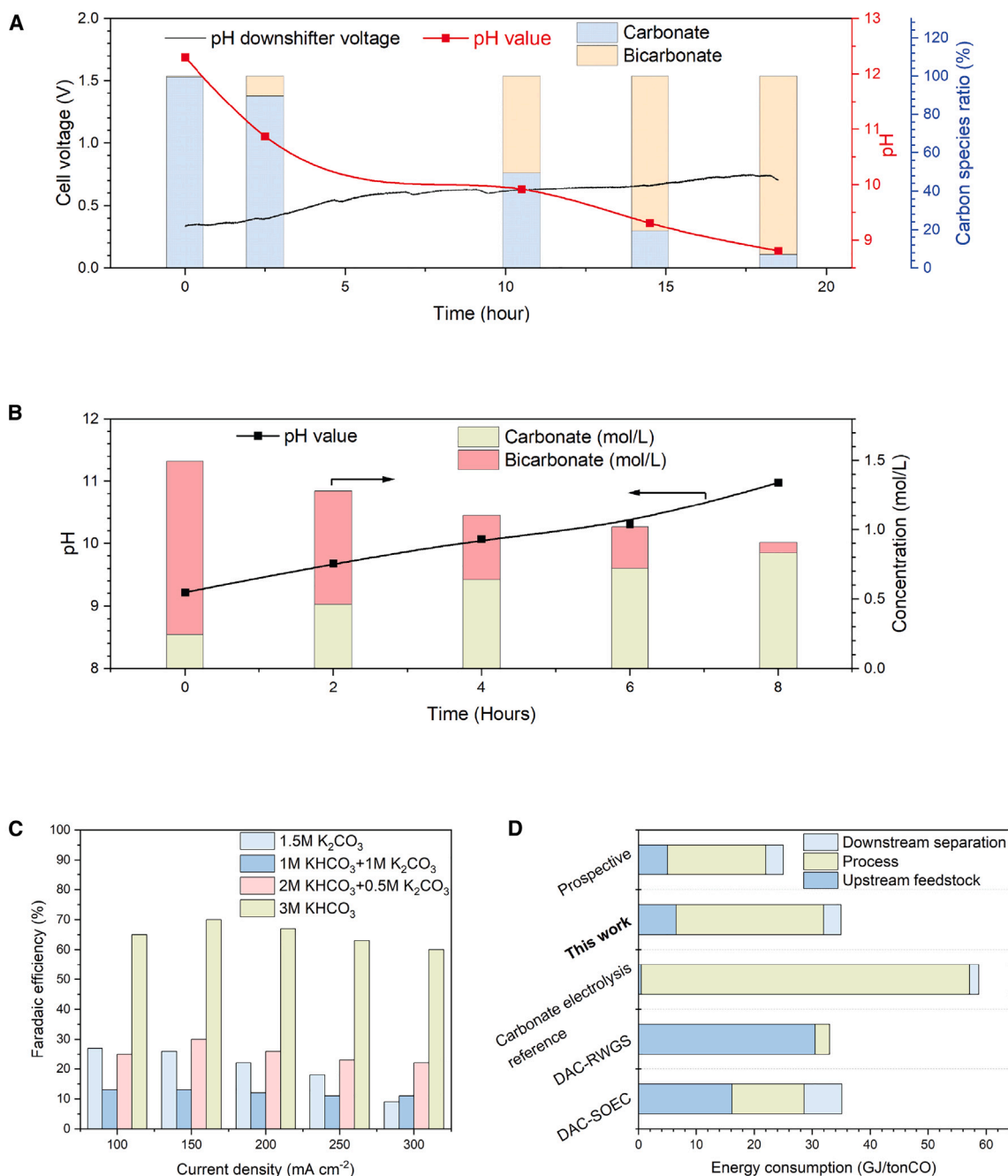


**Figure 4. System demonstration and energy assessment**

(A) Change of cell voltage, pH, and carbon species ratio, as a function of the duration of continuous operation of the pH-downshifter operating at a current density of 25 mA cm<sup>-2</sup>.

(B) Change of pH and (b) carbonate concentration as a function of the duration of continuous operation of the electrolyzer.

(C) The dependence of  $FE_{CO}$  on the input solution composition, where each solution is saturated using N<sub>2</sub>.

(D) Comparison among approaches to CO<sub>2</sub> to CO upgrade from dilute sources.

## METHODS

### Electrode preparation

All reagents used in this work were purchased from suppliers without further purification. Cobalt(II) 2,3-naphthalocyanine

was purchased from MilliporeSigma and cobalt(II) 2,9,16,23-tetra(carboxy)phthalocyanine was purchased from April Scientific. The CNTs, carboxylated CNT and amino CNT, were purchased from XFNANO. Nafion D520CS was ordered from Ion Power. Briefly, 200 mg of the CNTs were dispersed in 100 mL of

dimethylformamide (DMF) using sonication. Then, an appropriate amount (13 mg) of cobalt(II) phthalocyanine dissolved in 20 mL of DMF was added into the solution drop by drop, and the solution was stirred under 110°C for 12 h under reflux condenser. Afterward, the sample was filtered and washed with DMF several times to remove unreacted precursors. Then, the samples were freeze-dried and used for further experiments. This preparation procedure was applied to amide, carboxylate, control, amine, and amino-CoPc/CNT. No-linkage sample was prepared using the same methods without heating.

The catalyst ink was prepared by dispersing catalyst in methanol with added Nafion ionomer by ultrasonication. The ink was well sonicated for a good dispersion of catalyst. The mass ratio of the catalysts and ionomer was 1:1. The ink was then air-brushed onto the hydrophilic carbon substrate (Freudenberg H23, Fuel Cell Store) to the final loading of  $\sim 1.2 \text{ mg cm}^{-2}$ .

NiFeO<sub>x</sub> electrode was prepared with the following procedures. First, Ni foam was washed by 6 M HCl and deionized (DI) water for 15 min under sonication. Then, a 40-mL solution with 4 mmol NH<sub>4</sub>F, 10 mmol urea, 2 mmol Ni(NO<sub>3</sub>)<sub>2</sub>·6H<sub>2</sub>O, and 2 mmol Fe(NO<sub>3</sub>)<sub>3</sub>·9H<sub>2</sub>O was prepared and transferred to a 50-mL Teflon-lined stainless steel autoclave. The hydrothermal growth of the hydroxides on Ni foam was performed at 120°C for 6 h with a heating rate of 3°C min<sup>-1</sup>, followed by sonication in DI water and drying in the oven at 80°C.

### Electrochemical measurements

A cathode was cut into a 1.5 cm × 1.5 cm piece and placed onto the MEA cathode plate with a flow window with a dimension of 1 cm × 1 cm. Onto the cathode, a porous interposer layer (2 cm × 2 cm 85- $\mu\text{m}$ -thick PTFE) was carefully placed. When using the custom BPM, a TiO<sub>2</sub>-coated Nafion membrane was placed onto the porous interposer layer with the TiO<sub>2</sub> layer facing up, then covered by a PiperION (2 cm × 2 cm) membrane. A NiFeO<sub>x</sub> loaded Ni foam was placed onto the PiperION membrane as the anode. Two stainless steel flow-field plates with serpentine channels were used to sandwich the electrodes. The catholyte and anolyte were circulated by peristaltic pumps (INTLLAB) at 75 ml min<sup>-1</sup>. The applied current was controlled by an Autolab potentiostat/galvanostat. The membrane used to separate catholyte and anolyte was a commercial (Fumasep FBM, Fuel Cell Store) or custom-designed BPM. The pore size of the hydrophilic interposer layer was controlled at 0.1, 1, 5, and 10  $\mu\text{m}$  for PTFE membrane; 10, 20, and 41  $\mu\text{m}$  for nylon membrane; and 10  $\mu\text{m}$  for polyphenylene ether membrane. The catholyte was 3 M KHCO<sub>3</sub>, and the anolyte was 1 M KOH. All experiments were performed at room temperature.

CV was conducted by a general three-electrode configuration from -0.2 to 1.0 V (vs. RHE) at scan rate of 500 mV s<sup>-1</sup> in N<sub>2</sub>-saturated 3.0 M KHCO<sub>3</sub> electrolyte to observe the redox behavior of cobalt sites. The catalyst loading amount is 0.1 mg cm<sup>-2</sup>.

### Materials characterization

XPS was carried out on a Thermo Scientific NEXSA G2 XPS spectrometer, equipped with an Al K alpha radiation source and electron flood gun, at a pressure of  $8 \times 10^{-8}$  mbar with a pass energy of 50 eV. All spectra were calibrated with the C 1s

peak at 284.8 eV. Scanning electron microscopy-EDS (SEM-EDS) was conducted by JEOL JSM-7900FLV SEM at an accelerating voltage of 10 kV with backscattered electron detection, which is equipped with a light-element X-ray detector and an Oxford Aztec energy-dispersive X-ray analysis system. Aberration-corrected scanning transmission electron microscopy (STEM) images and EDS mappings were taken from taken using JEOL ARM200CF transmission electron microscopy (TEM) equipped with dual SDD EDS detector. For TEM sample was dispersed in ethanol followed by drop-casting on the grid.

*In situ* Raman analysis was conducted with a Renishaw inVia Raman spectrometer using an in-house *in situ* cell and a ×50 water immersion lens. Materials were coated on hydrophobic carbon paper as the cathode in electrolytes of 3 M KHCO<sub>3</sub>, purged with CO<sub>2</sub> from the back side. *In situ* analysis was performed in a flow cell having three compartments, with a Pt wire serving as anode. All potentials are referenced to Ag/AgCl.

### RESOURCE AVAILABILITY

#### Lead contact

Further information and requests for resources and materials should be directed to and will be fulfilled by the lead contact, Edward H. Sargent ([ted.sargent@northwestern.edu](mailto:ted.sargent@northwestern.edu)).

#### Materials availability

Further information and requests for resources and materials should be directed to and will be fulfilled by the [lead contact](#), Edward H. Sargent ([ted.sargent@northwestern.edu](mailto:ted.sargent@northwestern.edu)).

#### Data and code availability

The original data supporting the current study are available from the [lead contact](#) on request.

### ACKNOWLEDGMENTS

This work received support from Office of Naval Research under the agreement no. N00014-22-1-2690.

### AUTHOR CONTRIBUTIONS

E.H.S. and K.X. supervised the project. B.Z. and H.L. performed most of the electrochemical measurements, material synthesis, and characterization. G.S. carried out techno-economic analysis and life cycle assessment. H.S. carried out the electrochemical measurements. H.Z. and W.N. helped with the Raman spectroscopy measurements. B.P. performed HRTEM characterization. Y.L. and C.Y. helped with characterization. X.-Y.L., Y.C., and P.O. conducted DFT calculations. W.Z. helped with BPM fabrication. All authors discussed the results and contributed to writing and editing of the manuscript.

### DECLARATION OF INTERESTS

A patent disclosure was filed in Northwestern IP office (ID: Disc-ID-24-08-22-001).

### SUPPLEMENTAL INFORMATION

Supplemental information can be found online at <https://doi.org/10.1016/j.joule.2025.101883>.

Received: November 8, 2024

Revised: January 28, 2025

Accepted: February 28, 2025

Published: March 26, 2025

## REFERENCES

1. Siegel, R.E., Pattanayak, S., and Berben, L.A. (2023). Reactive Capture of CO<sub>2</sub>: Opportunities and Challenges. *ACS Catal.* **13**, 766–784. <https://doi.org/10.1021/acscatal.2c05019>.
2. Xia, Q., Zhang, K., Zheng, T., An, L., Xia, C., and Zhang, X. (2023). Integration of CO<sub>2</sub> Capture and Electrochemical Conversion. *ACS Energy Lett.* **8**, 2840–2857. <https://doi.org/10.1021/acsenerylett.3c00738>.
3. Carneiro, J.S.A., Innocenti, G., Moon, H.J., Guta, Y., Proaño, L., Sievers, C., Sakwa-Novak, M.A., Ping, E.W., and Jones, C.W. (2023). Insights into the Oxidative Degradation Mechanism of Solid Amine Sorbents for CO<sub>2</sub> Capture from Air: Roles of Atmospheric Water. *Angew. Chem. Int. Ed. Engl.* **62**, e202302887. <https://doi.org/10.1002/anie.202302887>.
4. Yu, X., Catanescu, C.O., Bird, R.E., Satagopan, S., Baum, Z.J., Lotti Diaz, L.M., and Zhou, Q.A. (2023). Trends in Research and Development for CO<sub>2</sub> Capture and Sequestration. *ACS Omega* **8**, 11643–11664. <https://doi.org/10.1021/acsomega.2c05070>.
5. De Luna, P., Hahn, C., Higgins, D., Jaffer, S.A., Jaramillo, T.F., and Sargent, E.H. (2019). What would it take for renewably powered electrosynthesis to displace petrochemical processes? *Science* **364**, eaav3506. <https://doi.org/10.1126/science.aav3506>.
6. Liu, S., Zhang, J., Li, F., Edwards, J.P., Xiao, Y.C., Kim, D., Papangelakis, P., Kim, J., Elder, D., De Luna, P., et al. (2024). Direct air capture of CO<sub>2</sub> via cyclic viologen electrocatalysis. *Energy Environ. Sci.* **17**, 1266–1278. <https://doi.org/10.1039/D3EE03024E>.
7. Xu, Y., Liu, S., Edwards, J.P., Xiao, Y.C., Zhao, Y., Miao, R.K., Fan, M., Chen, Y., Huang, J.E., Sargent, E.H., et al. (2023). Regeneration of direct air CO<sub>2</sub> capture liquid via alternating electrocatalysis. *Joule* **7**, 2107–2117. <https://doi.org/10.1016/j.joule.2023.07.011>.
8. Keith, D.W., Holmes, G., St. Angelo, D., and Heidel, K. (2018). A Process for Capturing CO<sub>2</sub> from the Atmosphere. *Joule* **2**, 1573–1594. <https://doi.org/10.1016/j.joule.2018.05.006>.
9. Chowdhury, S., Kumar, Y., Shrivastava, S., Patel, S.K., and Sangwai, J.S. (2023). A Review on the Recent Scientific and Commercial Progress on the Direct Air Capture Technology to Manage Atmospheric CO<sub>2</sub> Concentrations and Future Perspectives. *Energy Fuels* **37**, 10733–10757. <https://doi.org/10.1021/acs.energyfuels.2c03971>.
10. Liu, G., Hu, Z., and Lisak, G. (2024). CO<sub>2</sub> capture and utilization through isothermal carbonation-calcination looping integrated with MSW pyrolysis volatile reforming. *Chem. Eng. J.* **482**, 149164. <https://doi.org/10.1016/j.cej.2024.149164>.
11. Lee, G., Rasouli, A.S., Lee, B.-H., Zhang, J., Won, D.H., Xiao, Y.C., Edwards, J.P., Lee, M.G., Jung, E.D., Arabyarmohammadi, F., et al. (2023). CO<sub>2</sub> electroreduction to multicarbon products from carbonate capture liquid. *Joule* **7**, 1277–1288. <https://doi.org/10.1016/j.joule.2023.05.003>.
12. Kar, S., Rahaman, M., Andrei, V., Bhattacharjee, S., Roy, S., and Reisner, E. (2023). Integrated capture and solar-driven utilization of CO<sub>2</sub> from flue gas and air. *Joule* **7**, 1496–1514. <https://doi.org/10.1016/j.joule.2023.05.022>.
13. Office of Fossil Energy and Carbon Management (2025). Carbon Conversion. <https://www.energy.gov/fecm/carbon-conversion>.
14. Almajed, H.M., Kas, R., Brimley, P., Crow, A.M., Somoza-Tornos, A., Hodge, B.M., Burdyny, T.E., and Smith, W.A. (2024). Closing the loop: Unexamined Performance Trade-Offs of Integrating Direct Air Capture with (Bi)carbonate Electrolysis. *ACS Energy Lett.* **9**, 2472–2483. <https://doi.org/10.1021/acsenerylett.4c00807>.
15. Li, Y.C., Lee, G., Yuan, T., Wang, Y., Nam, D.-H., Wang, Z., García de Arquer, F.P., Lum, Y., Dinh, C.-T., Voznyy, O., et al. (2019). CO<sub>2</sub> Electroreduction from Carbonate Electrolyte. *ACS Energy Lett.* **4**, 1427–1431. <https://doi.org/10.1021/acsenerylett.9b00975>.
16. Xiao, Y.C., Gabardo, C.M., Liu, S., Lee, G., Zhao, Y., O'Brien, C.P., Miao, R.K., Xu, Y., Edwards, J.P., Fan, M., et al. (2023). Direct carbonate electroreduction into pure syngas. *EES. Catal.* **1**, 54–61. <https://doi.org/10.1039/D2EY00046F>.
17. Shen, M., Ji, L., Cheng, D., Wang, Z., Xue, Q., Feng, S., Luo, Y., Chen, S., Wang, J., Zheng, H., et al. (2024). Hierarchical design enables sufficient activated CO<sub>2</sub> for efficient electrolysis of bicarbonate to CO. *Joule* **8**, 1999–2015. <https://doi.org/10.1016/j.joule.2024.04.006>.
18. Song, H., Fernández, C.A., Choi, H., Huang, P.-W., Oh, J., and Hatzell, M.C. (2024). Integrated carbon capture and CO production from bicarbonates through bipolar membrane electrolysis. *Energy Environ. Sci.* **17**, 3570–3579. <https://doi.org/10.1039/D4EE00048J>.
19. Lawson, S.E., Roberts, R.J., Leznoff, D.B., and Warren, J.J. (2024). Dramatic Improvement of Homogeneous Carbon Dioxide and Bicarbonate Electroreduction Using a Tetracationic Water-Soluble Cobalt Phthalocyanine. *J. Am. Chem. Soc.* **146**, 22306–22317. <https://doi.org/10.1021/jacs.4c04878>.
20. Feng, S., Wang, X., Cheng, D., Luo, Y., Shen, M., Wang, J., Zhao, W., Fang, S., Zheng, H., Ji, L., et al. (2024). Stabilizing \*CO<sub>2</sub> Intermediates at the Acidic Interface using Molecularly Dispersed Cobalt Phthalocyanine as Catalysts for CO<sub>2</sub> Reduction. *Angew. Chem. Int. Ed. Engl.* **63**, e202317942. <https://doi.org/10.1002/anie.202317942>.
21. Zhang, X., Wu, Z., Zhang, X., Li, L., Li, Y., Xu, H., Li, X., Yu, X., Zhang, Z., Liang, Y., et al. (2017). Highly selective and active CO<sub>2</sub> reduction electrocatalysts based on cobalt phthalocyanine/carbon nanotube hybrid structures. *Nat. Commun.* **8**, 14675. <https://doi.org/10.1038/ncomms14675>.
22. Rooney, C.L., Lyons, M., Wu, Y., Hu, G., Wang, M., Choi, C., Gao, Y., Chang, C.W., Brudvig, G.W., Feng, Z., et al. (2024). Active Sites of Cobalt Phthalocyanine in Electrocatalytic CO<sub>2</sub> Reduction to Methanol. *Angew. Chem. Int. Ed. Engl.* **63**, e202310623. <https://doi.org/10.1002/anie.202310623>.
23. Wang, M., Torbensen, K., Salvatore, D., Ren, S., Joulié, D., Dumoulin, F., Mendoza, D., Lassalle-Kaiser, B., Işci, U., Berlinguette, C.P., et al. (2019). CO<sub>2</sub> electrochemical catalytic reduction with a highly active cobalt phthalocyanine. *Nat. Commun.* **10**, 3602. <https://doi.org/10.1038/s41467-019-11542-w>.
24. Zhou, S., Zhang, L.J., Zhu, L., Tung, C.H., and Wu, L.Z. (2023). Amphiphilic Cobalt Phthalocyanine Boosts Carbon Dioxide Reduction. *Adv. Mater.* **35**, e2300923. <https://doi.org/10.1002/adma.202300923>.
25. Xu, H., Cai, H., Cui, L., Yu, L., Gao, R., and Shi, C. (2023). Molecular modulation of cobalt phthalocyanines on amino-functionalized carbon nanotubes for enhanced electrocatalytic CO<sub>2</sub> conversion. *Nano Res.* **16**, 3649–3657. <https://doi.org/10.1007/s12274-022-4578-x>.
26. Ren, S., Lees, E.W., Hunt, C., Jewlial, A., Kim, Y., Zhang, Z., Mowbray, B.A.W., Fink, A.G., Melo, L., Grant, E.R., et al. (2023). Catalyst Aggregation Matters for Immobilized Molecular CO<sub>2</sub>RR Electrocatalysts. *J. Am. Chem. Soc.* **145**, 4414–4420. <https://doi.org/10.1021/jacs.2c08380>.